



## OPEN ACCESS

## EDITED BY

Hakan Arslan,  
Mersin University, Türkiye

## REVIEWED BY

Elvan Üstün,  
Ordu University, Türkiye  
Yang Wei,  
Boston College, United States

## \*CORRESPONDENCE

Samar A. Aly,  
✉ samar.mostafa@gebri.usc.edu.eg  
Ahlam I. Al-Sulami,  
✉ aialsulami@uj.edu.sa  
Ehab M. Abdalla,  
✉ Ehababdalla99@sci.nvu.edu.eg

RECEIVED 17 December 2023

ACCEPTED 22 January 2024

PUBLISHED 12 February 2024

## CITATION

Hassan SS, Aly SA, Al-Sulami AI, Albohy SAH,  
Salem MF, Nasr GM and Abdalla EM (2024),  
Synthesis, characterization, PXRD studies, and  
theoretical calculation of the effect of gamma  
irradiation and antimicrobial studies on novel  
Pd(II), Cu(II), and Cu(I) complexes.  
*Front. Chem.* 12:1357330.  
doi: 10.3389/fchem.2024.1357330

## COPYRIGHT

© 2024 Hassan, Aly, Al-Sulami, Albohy, Salem,  
Nasr and Abdalla. This is an open-access article  
distributed under the terms of the [Creative  
Commons Attribution License \(CC BY\)](#). The use,  
distribution or reproduction in other forums is  
permitted, provided the original author(s) and  
the copyright owner(s) are credited and that the  
original publication in this journal is cited, in  
accordance with accepted academic practice.  
No use, distribution or reproduction is  
permitted which does not comply with these  
terms.

# Synthesis, characterization, PXRD studies, and theoretical calculation of the effect of gamma irradiation and antimicrobial studies on novel Pd(II), Cu(II), and Cu(I) complexes

Safaa S. Hassan<sup>1</sup>, Samar A. Aly<sup>2\*</sup>, Ahlam I. Al-Sulami<sup>3\*</sup>,  
Salwa A. H. Albohy<sup>4</sup>, Mohamed F. Salem<sup>2</sup>, Ghada M. Nasr<sup>5</sup> and  
Ehab M. Abdalla<sup>6\*</sup>

<sup>1</sup>Chemistry Department, Faculty of Science, Cairo University, Giza, Egypt, <sup>2</sup>Department of Environmental Biotechnology, Genetic Engineering and Biotechnology Research Institute, University of Sadat City, Sadat, Egypt, <sup>3</sup>Department of Chemistry, College of Science, University of Jeddah, Jeddah, Saudi Arabia, <sup>4</sup>Chemistry Department, Faculty of Science (Girls), Al-Azhar University, Nasr, Cairo, Egypt, <sup>5</sup>Department of Molecular Diagnostics and Therapeutics, Genetic Engineering and Biotechnology Research Institute, University of Sadat City, Sadat, Egypt, <sup>6</sup>Chemistry Department, Faculty of Science, New Valley University, El-Kharga, Egypt

The main objective of this study is to synthesize and characterize of a new three complexes of Pd (II), Cu (II), and Cu (I) metal ions with novel ligand ((Z)-2-(phenylamino)-N'-(thiophen-2-ylmethylene)acetohydrazide) H<sub>2</sub>L<sub>B</sub>. The structural composition of new compounds was assessed using several analytical techniques including FT-IR, <sup>1</sup>H-NMR, electronic spectra, powder X-ray diffraction, and thermal behavior analysis. The Gaussian09 program employed the Density Functional Theory (DFT) approach to optimize the geometry of all synthesized compounds, therefore obtaining the most favorable structures and crucial parameters. An investigation was conducted to examine the impact of  $\gamma$ -irradiation on ligands and complexes. Before and after  $\gamma$ -irradiation, the antimicrobial efficiency was investigated for the activity of ligands and their chelates. The Cu(I) complex demonstrated enhanced antibacterial activity after irradiation, as well as other standard medications such as ampicillin and gentamicin. Similarly, the Cu(I) complex exhibited superior activity against antifungal species relative to the standard drug Nystatin. The docking investigation utilized the target location of the topoisomerase enzyme (2xct) chain A.

## KEYWORDS

complexes,  $\gamma$ -irradiation, antimicrobial, thermal, DFT, molecular docking

## 1 Introduction

Hydrazone derivatives are a large class of chemicals used in various medicinal applications (Abdalla et al., 2021) because of their broad range of pharmacokinetic features (Popiołek et al., 2018; Aneja et al., 2019; El-saied et al., 2020; Katariya et al., 2020), particularly in drug detection programmers. The hydrazone and carbaldehyde

TABLE 1 Physicochemical parameters of all compounds.

No.	Compounds Molecular Formula	M.Wt	Color Yield %	$\wedge m$	$\mu_{eff}/BM$	(Cal.) Found %			
						C	H	N	M
H <sub>2</sub> L <sub>B</sub>	C <sub>15</sub> H <sub>15</sub> N <sub>3</sub> O <sub>4</sub>	301.30	Yellow 74	—	—	59.80 (59.76)	5.02 (4.98)	13.95 (13.92)	—
B <sub>1</sub>	Pd(H <sub>2</sub> L) <sub>2</sub> ]Cl <sub>2</sub> ·2H <sub>2</sub> O C <sub>30</sub> H <sub>34</sub> Cl <sub>2</sub> N <sub>6</sub> O <sub>10</sub> Pd	815.95	Orange 70	65	Dia	44.16 (44.03)	4.20 (4.11)	10.30 (10.21)	13.04 (12.96)
B <sub>2</sub>	Cu(H <sub>2</sub> L) <sub>2</sub> Br <sub>2</sub> C <sub>30</sub> H <sub>30</sub> Br <sub>2</sub> CuN <sub>6</sub> O <sub>8</sub>	825.96	Green 76	25	1.74	43.63(43.57)	3.66 (3.58)	10.18 (10.09)	7.69 (7.61)
B <sub>3</sub>	Cu(H <sub>2</sub> L)Cl C <sub>15</sub> H <sub>15</sub> ClCuN <sub>3</sub> O <sub>4</sub>	400.30	Green 72	30	Dia	45.01 (44.96)	3.78 (3.74)	10.50 (10.43)	15.87 (15.82)

Where:  $\wedge m$  = molar conductivity (ohm<sup>-1</sup>, cm<sup>2</sup> mol<sup>-1</sup>) in 10<sup>-3</sup> M DMF, solution.

TABLE 2 FT- IR spectral bands all compounds before (B) and after (A) irradiation in 4,000–400 cm<sup>-1</sup>, A = After irradiation and B = Before irradiation.

No.	Compound	$\nu(OH/H_2O)$	$\nu(N-H)$	$\nu(C=O)_{side}$	$\nu(C=O)_{ring}$	$\nu(C=N)$	$\nu(M-O)$	$\nu(M-N)$
H <sub>2</sub> L <sub>B</sub> H <sub>2</sub> L <sub>A</sub>	C <sub>15</sub> H <sub>15</sub> N <sub>3</sub> O <sub>4</sub>	3,392 3,391	3,202 3,202	1,677 1,675	1,639 1,635	1,604 1,600	—	—
DFT		3,595	3,244	1,700	1,633	1,597	—	—
B <sub>1</sub> A <sub>1</sub>	[Pd(H <sub>2</sub> L) <sub>2</sub> ]Cl <sub>2</sub> ·2H <sub>2</sub> O	3,435 3,434	2,921 2,917	1,687 1,685	1,625 1,621	1,545 1,547	603 600	539 545
DFT		3,424	3,046	1,669	1,642	1,552	598	535
B <sub>2</sub> A <sub>2</sub>	Cu(H <sub>2</sub> L) <sub>2</sub> Br <sub>2</sub>	3,440 3,490	3,251 3,205	1,696 1,698	1,601 1,600	1,550 1,548	537 536	485 479
DFT		3,487	3,280	1,696	1,624	1,561	535	490
B <sub>3</sub> A <sub>3</sub>	Cu(H <sub>2</sub> L)Cl	3,490 3,487	3,188 3,191	1,695 1,693	1,602 1,601	1,550 1,550	537 579	508 513
DFT		3,500	3,199	1,687	1,597	1,552	589	517

TABLE 3 Electronic spectra data of all compounds before (H<sub>2</sub>L<sub>B</sub>, B<sub>1</sub>- B<sub>3</sub>) and after (H<sub>2</sub>L<sub>A</sub>, A<sub>1</sub>- A<sub>3</sub>) irradiation.

No	Compound	$\lambda_{max}(nm)$	DFT
H <sub>2</sub> L <sub>B</sub> H <sub>2</sub> L <sub>A</sub>	H <sub>2</sub> L	341, 399 335, 394	310,430
B <sub>1</sub>	Pd(H <sub>2</sub> L) <sub>2</sub> ]Cl <sub>2</sub> ·2H <sub>2</sub> O	332,393, 511	650
A <sub>1</sub>		326,389, 502	
B <sub>2</sub>	Cu(H <sub>2</sub> L) <sub>2</sub> Br <sub>2</sub>	352, 399, 571	620
A <sub>2</sub>		346, 394, 563	
B <sub>3</sub>	Cu(H <sub>2</sub> L)Cl	343, 399, 487, 615	450, 460, 600
A <sub>3</sub>		331, 397, 469, 595	

derivatives, as well as their complexes, have been reported to reveal a wide range of biological features (Sepay and Dey, 2014; Parveen et al., 2018; Naveen et al., 2020; Zülfikaroglu et al., 2020), such as anticancer (Mandewale et al., 2017; Manohar et al., 2018; Yousefi et al., 2019; Babahan et al., 2020), antibacterial (Ekennia et al., 2018; Özbek et al., 2019; Khan et al., 2020), antimicrobial (Cao et al., 2018; Philip et al., 2018; Santiago et al., 2020), antifungal (Rocha et al., 2019; Elsayed et al., 2020), antimalarial (Maurya et al., 2017), antiviral (Sreepriya et al., 2020), antimycobacterial (Mandewale et al., 2017; Mandewale

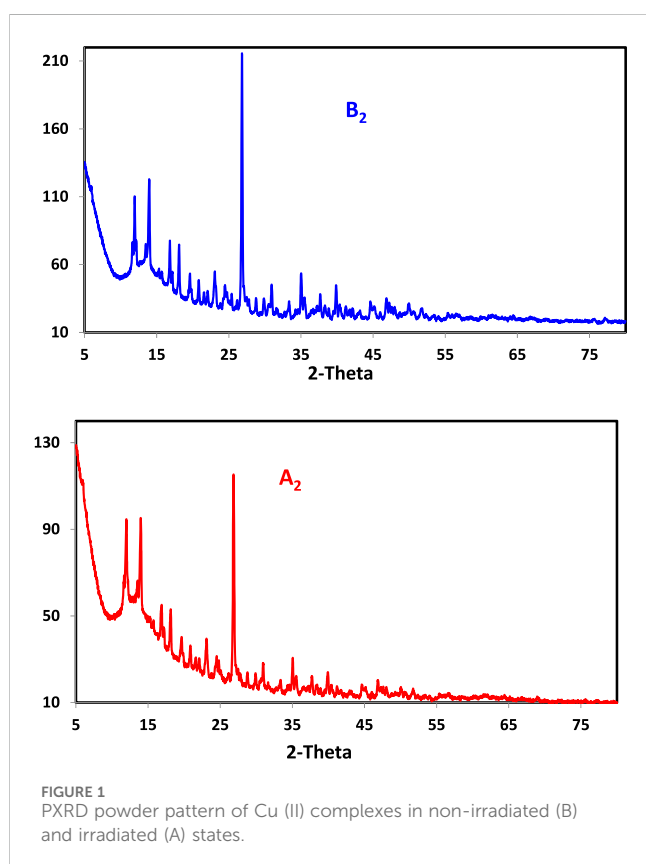
et al., 2018), antileishmanial (Coimbra et al., 2019), antiplatelet (Margariti et al., 2020), anti-analgesic antitubercular, anticonvulsant (Dehestani et al., 2018), anti-uropathogenic (Alodeani et al., 2015), antiproliferative (Bergamini et al., 2019), antiarthritic (Shabbir et al., 2014), and antioxidant properties (Vanucci-Bacqué et al., 2016; Anastassova et al., 2018; Al-Hazmi et al., 2020); potent immunomodulatory agents (Meira et al., 2018); and potent antiangiogenic agents in atherosclerosis (Vanucci-Bacqué et al., 2016). They are also essential in Alzheimer's disease treatment (Haghighijoo et al., 2017; Parlar et al., 2019).

Garoufis et al. evaluated several scholarly studies on the antibacterial, antiviral, and antifungal properties of Pd II) chelates with diverse ligands (Other ligands include nitrogen and sulfur donor sites, Schiff base ligands, and other medications) (Guerra et al., 2005; Garoufis et al., 2009). Other studies have recently been published in the literature that revealed diverse palladium complex activity intensities on distinct bacteria and fungus species (Aghatabay et al., 2007; Biyala et al., 2008; Vieira et al., 2009).

Copper is the primary component of copper doorknobs and touch surfaces in hospitals and healthcare facilities that prevent bacteria and diseases from growing and spreading ("contact killing") (Tian et al., 2012). Many copper complexes with potential and diverse biological action have been discovered in the literature, including antibacterial (Beeton et al., 2014; Lobana

TABLE 4 PXRD data of ligand and chelates (B) before and (A) after irradiation.

Compound	Angle 2θ	d- value nm	FWHM	Grain size Nm
H <sub>2</sub> L <sub>B</sub>	15.822	0.559119	0.238	37.48
H <sub>2</sub> L <sub>A</sub>	15.801	0.558271	0.262	31.99
B <sub>2</sub>	26.321	0.332158	0.167	51.64
A <sub>2</sub>	26.400	0.331720	0.213	40.25



et al., 2014), anticancer (Qiu et al., 2015; Stefani et al., 2015), anticonvulsant (Lemoine et al., 2002), antifungal (Soroceanu et al., 2016), anti-inflammatory (Hoonur et al., 2010), antimalarial (Hubin et al., 2014), anti-neurodegenerative (Quintanova et al., 2015), antiobesity (Perontsis et al., 2016), antioxidant (Tolia et al., 2013), anti-rheumatic (Sherif and Hosny, 2014), antithyroid (Urquiza et al., 2015), antitubercular (Netalkar et al., 2014), and antiviral activity (Dorotíková et al., 2015).

Radiation is widely used in biomaterials science to alter surface properties, clean surfaces, and improve bulk properties. In addition to biochips and situ photopolymerizable biogluers, radiation is used to develop biochips (Aly and Elembaby, 2020b). Gamma radiation, great-energy electrons, and ultraviolet radiation are the most common energy sources used to irradiate biomaterials (Balashova et al., 2019; Aly et al., 2022a; Elganzory et al., 2022). The manuscript aimed to prepare, characterize, and investigate the impact of gamma irradiation

on Pd(II), Cu(II), and Cu(I) metal complexes and also an antimicrobial study of these compounds.

## 2 Experimental method

### 2.1 Synthesis of hydrazone ligand

First, 20 mL of ultra-grade ethanol was added to a round flask along with 0.01 mol of 2-(p-tolylamino)acetohydrazide and 0.01 mol of 5-hydroxy-4-oxo-4H-pyran-3-carbaldehyde. The resultant liquid was mixed for approximately 6 h at room temperature (Abdalla et al., 2021). The resulting precipitate was separated after washing and drying into a filter paper. The washing solutions were ethyl alc and diethyl ether (Aly et al., 2021).

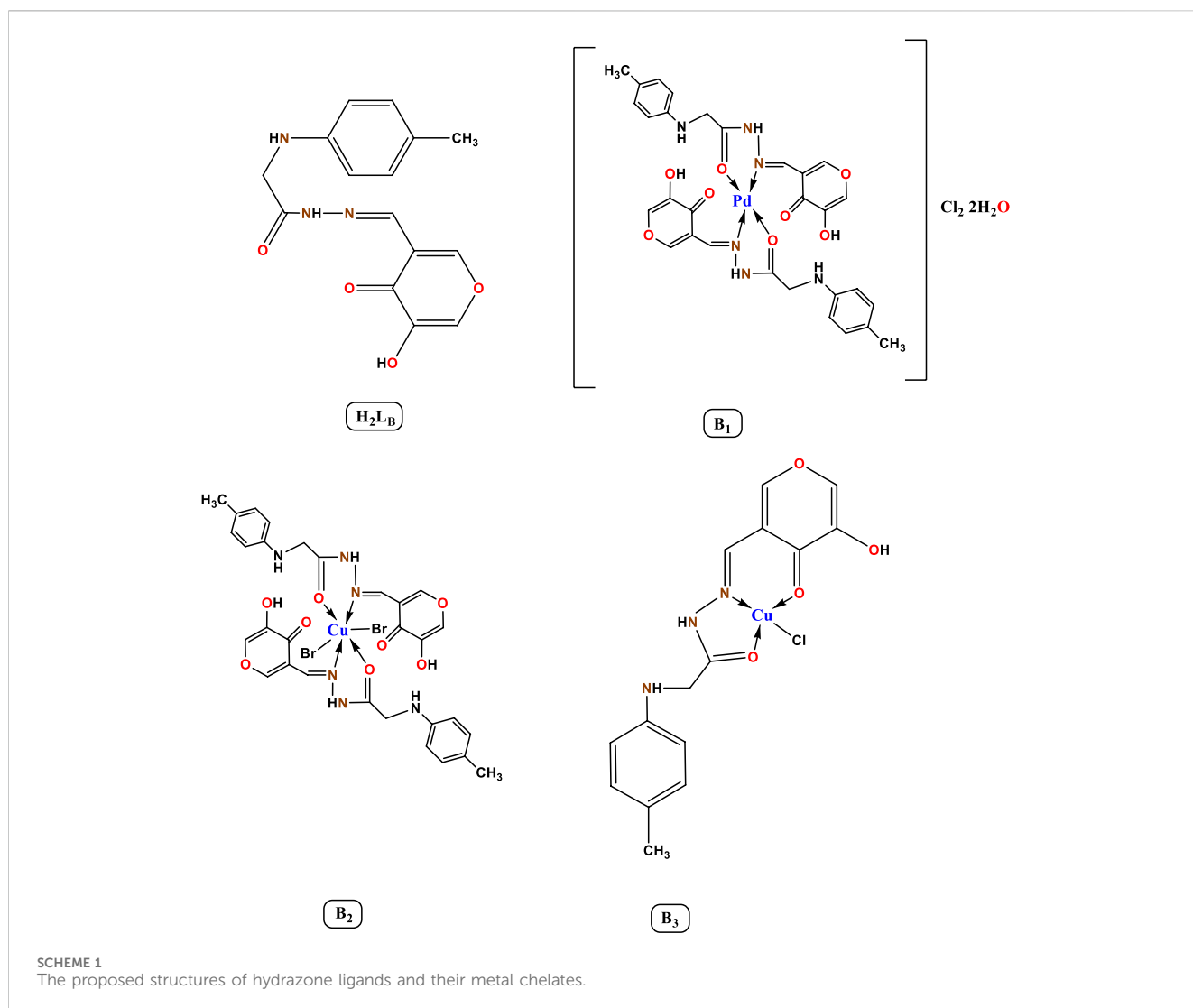
C<sub>15</sub>H<sub>15</sub>N<sub>3</sub>O<sub>4</sub> (H<sub>2</sub>L<sub>B</sub>): Yellow, Molecular Weight: 301.3, Yield = 94%; Analytical Calculated: H, 5.02; C, 59.80; N, 13.95. Exp. (%):H, 4.98; C, 59.76; N, 13.92. The FTIR bands (cm<sup>-1</sup>) at 3,392, 3,202, 1,677, 1,639, and 1,604 related to (OH/H<sub>2</sub>O), (N-H), (C=O)<sub>side</sub>, and (C=N) respectively. Electronic transitions: λ<sub>max</sub>: 341, 399. <sup>1</sup>HNMR: δ (ppm): 2.10, 3.91, 5.84–6.63, 7.11, 11.10, and 15.90 were related to (s, 3H, CH<sub>3</sub>), (s, 2H, NCH<sub>2</sub>), (s, 1H, NH), (s, 1H, NCH), (m, 4H, p-sub. Ph-H), (s, 2H, pyran-H), (bs, 1H, NHC = O) and (bs, 1H, OH) respectively. <sup>13</sup>CNMR: δ (ppm): 19.2, 45.3, 148.2, (116.7, 128.7, 163.1, 169.1, 170.5), (112.4, 116.4, 128.8, 148.1) and 181.5 corresponded to (CH<sub>3</sub>), (NCH<sub>2</sub>), (C=N), (pyran-C), (Ph-C) and (C=O) respectively. Supplementary Figure S2.

### 2.2 Synthesis of metal complexes

According to a standard approach (Scheme 1), the metal salt was added to the ligand with a stoichiometric quantity (1 mmol; = 0.177 g Pd II); 0.099 g Cu(I); 0.223 g Cu(II) to 1 mmol = 0.301 of ligand). The solvent used was EtOH (20 mL). The reaction mixture was refluxed for 6 hours while stirring at 60°C. The colorful reaction product that resulted from the reaction was filtered out of the reaction mixture, extensively cleaned with ethyl alc to eliminate the unreacted starting residues, and vacuum-dried (Frisch et al., 2009a). TLC was used to verify the complexes' purity.

### 2.3 Analytical and physical measurements

All of the starting materials used in this investigation (which were of analytical quality and were not purified before use) were provided by Sigma-Aldrich and Fluka. Detailed information on the



tools and procedures used for structure confirmation and application are provided in the [Supplementary Material](#).

## 2.4 Quantum chemical calculation QCC

GaussView 5.0.8 (Wallingford, CT 2009) (Frisch et al., 2009a) was used to prepare the input files of compounds. Gaussian 09 rev. A.02 was used for all computations (Wallingford, CT, 2009) (Frisch et al., 2009b). The DFT/B3LYP technique was used. The standard basis sets were 6311G and LANL2DZ concerning the synthesized H<sub>2</sub>L and its metal complexes, respectively (Ammar et al., 2014; Maurya et al., 2015; Ding et al., 2018; Abdalrazaq et al., 2022; Aly et al., 2022b; Mahani and Mohammadi, 2022; Ugurlu and Harmankaya, 2022). The topoisomerase IIa was simulated using MOE 2009 (Molecular Operating Environment) software. The topoisomerase II DNA gyrase protein crystal structure (PDB ID: 2XCT) was downloaded from the protein data bank. The docking steps involved constructing the investigated compounds using Chembio3D-ultra software followed by their optimization. The selected protein was downloaded from Protein Data Bank PDB. Finally, the binding affinity of each compound to the protein was evaluated.

## 2.5 Assay for antimicrobials

The antibacterial activity of the generated compounds was evaluated using the agar well diffusion method as reported in detail (Abdalla et al., 2020; Al-Farhan et al., 2021) and specifics of the antimicrobial screening process are provided in the [Supplementary Material](#).

## 2.6 Irradiation studies

Solid ligand and chelate complex samples were submitted to irradiation tests at a dosage of 60 kGy (Aly and Elembaby, 2020a) [Supplementary Section S3](#).

# 3 Result and discussion

## 3.1 Characterization

The chelates' analytical results confirmed the predicted chemical formulae and demonstrated the formation of 1:2 of Pd(II) and 1:1 of Cu(II) and Cu(I) (M:L) (Table 1). The molar conductance values

TABLE 5 Thermal data of all compounds before (B) and after (A) irradiation.

Compound		Temp. range/°C TGA	Mass loss% Calc.F)	Leaving species
C <sub>15</sub> H <sub>15</sub> N <sub>3</sub> O <sub>4</sub>	H <sub>2</sub> L <sub>B</sub>	197–250	51.4 (51.18)	C <sub>6</sub> H <sub>6</sub> N <sub>2</sub> O <sub>3</sub> C <sub>4</sub> H <sub>4</sub> C <sub>5</sub> H <sub>5</sub> NO
Residue		250–430	17.27 (17.30)	
		>430	31.55 (31.51)	
C <sub>15</sub> H <sub>15</sub> N <sub>3</sub> O <sub>4</sub>	H <sub>2</sub> L <sub>A</sub>	197–250	40.59 (40.53)	C <sub>6</sub> H <sub>6</sub> N <sub>2</sub> O C <sub>4</sub> H <sub>4</sub> NO <sub>2</sub> C <sub>5</sub> H <sub>5</sub> O
Residue		250–501	32.51 (32.55)	
		>501	26.87 (26.91)	
C <sub>30</sub> H <sub>34</sub> Cl <sub>2</sub> N <sub>6</sub> O <sub>10</sub> Pd	B <sub>1</sub>	45–225	13.27 (13.35)	2H <sub>2</sub> O+2HCl
Residue	A <sub>1</sub>	225–386	71.59 (71.64)	C <sub>30</sub> H <sub>28</sub> N <sub>6</sub> O <sub>7</sub>
			14.94 (15.00)	
		>386	13.32 (13.35)	
			71.61 (71.64)	
			14.97 (15.00)	
C <sub>30</sub> H <sub>30</sub> Br <sub>2</sub> CuN <sub>6</sub> O <sub>8</sub>	B <sub>2</sub>	30–210	19.53 (19.59)	2HBr
	A <sub>2</sub>	210–305	23.13 (23.03)	C <sub>10</sub> H <sub>12</sub> N <sub>3</sub> O
		305–591	47.71 (47.74)	C <sub>20</sub> H <sub>16</sub> N <sub>3</sub> O <sub>6</sub>
		>591	9.60 (9.63)	CuO
	Residue		30–191	9.76 (9.79)
191–461			34.91 (34.88)	C <sub>10</sub> H <sub>14</sub> N <sub>3</sub> O <sub>2</sub> Br
461–610			47.53 (47.50)	C <sub>20</sub> H <sub>14</sub> N <sub>3</sub> O <sub>6</sub>
>610			7.65 (7.69)	Cu
C <sub>15</sub> H <sub>15</sub> ClCuN <sub>3</sub> O <sub>4</sub>	B <sub>3</sub>	100–198	9.09 (9.12)	HCl
		198–495	38.21 (38.25)	C <sub>6</sub> H <sub>5</sub> N <sub>2</sub> O <sub>3</sub>
Residue	A <sub>3</sub>	495–571	36.83 (36.76)	C <sub>9</sub> H <sub>9</sub> NO
		>571	15.84 (15.87)	Cu

were measured in 10<sup>-3</sup> M DMF for the Cu (II), Cu(I), and Pd(II) complexes to give 25, 30, and 65 Ω<sup>-1</sup>cm<sup>2</sup>mol<sup>-1</sup> respectively. This result revealed that the Cu(II) and Cu(I) chelates were non-electrolytic (Aly and Fathalla, 2020); on the other hand, the Pd(II) complex was electrolytic.

### 3.2 <sup>1</sup>H- NMR interpretation of the non-irradiated and radiated ligands

(H<sub>2</sub>L) <sup>1</sup>H-NMR spectra in DMSO-*d*<sub>6</sub> (defining each ligand before and after irradiation) were confirmed. After radiation exposure, the signals stayed in the same spot or slightly moved in the ligand's <sup>1</sup>H-NMR spectrum (Supplementary Figure S1). Even yet, the bands' strength after irradiation was greater than before. The <sup>1</sup>H-NMR spectrum of the NH proton had a singlet signal at 5.94 ppm and a wide single peak at 11.1 ppm that identified the NHC = O proton in the hydrazone linkage. The spectral signature of aromatic ring protons also included a multiple signal between 6.70 and 6.75 ppm. The spectrum also exhibited singlet signals at

7.11 ppm, which were pyrene proton signals, and a wide single peak at 15.90 ppm, a hydroxyl group C-OH proton signal.

### 3.3 FT-IR spectra

Table 2 and Supplementary Figures S3-S6 clarify the IR spectra of the irradiated (A) and non-irradiated (B) states of H<sub>2</sub>L and its metal chelates. The IR spectra of H<sub>2</sub>L<sub>B</sub> and H<sub>2</sub>L<sub>A</sub> have revealed bands at 3,392, 3,391; 1,677, 1,675; 1,639, 1,635; and 1,604, 1,600 cm<sup>-1</sup> which corresponded to the Hydroxyl group, ν(carbonyl)<sub>side, ring</sub> and ν(C=N) for the non-irradiated and irradiated states respectively. Upon complexation, these bands were shifted to a higher or lower value where the band related to ν(OH) was shifted to higher values as in the Pd(II), Cu(II), and Cu(I) chelates exhibited at 3,435, 3,434; 3,440, 3,490 and 3,490, 3,487 cm<sup>-1</sup>, respectively. The ν(C=N) bands were changed at higher frequency after irradiation and were displayed at 1,545, 1,547; 1,550, 1,548; and 1,550 cm<sup>-1</sup>, respectively. The bands exhibited at 1,687, 1,685; 1,696, 1,698; and 1,695, 1,693 cm<sup>-1</sup> related to ν(OH) and ν(C=O)<sub>side</sub>

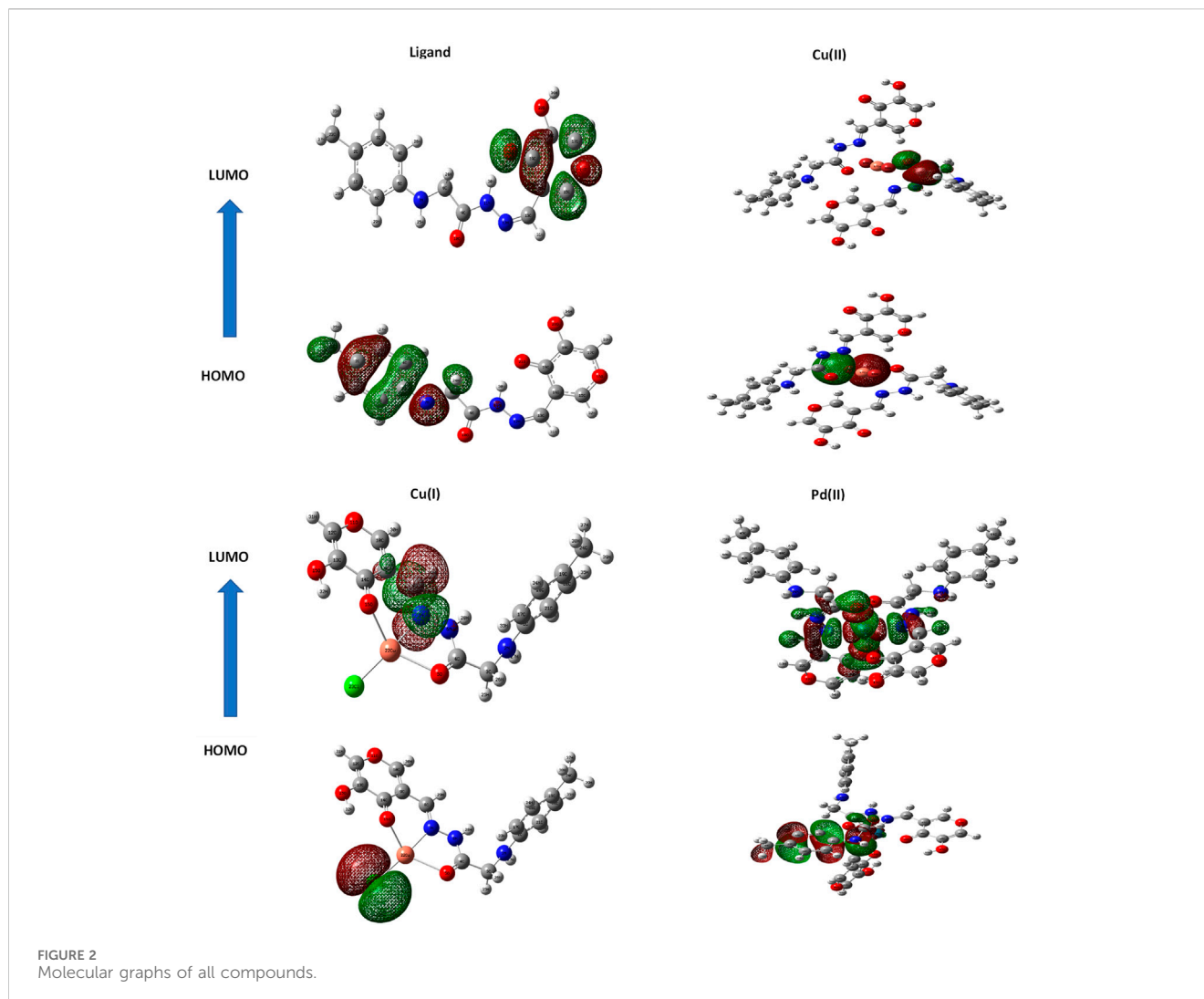


TABLE 6 Ground state criteria of ligand and Cu(I), Cu(II), and Pd(II) complexes using B3LYP/6-311G and B3LYP/LANL2DZ, respectively.

Parameter	H <sub>2</sub> L <sub>B</sub>	Cu(I) complex	Cu(II) complex	Pd(II) complex
E <sub>T</sub> , Hartree	-1,045.39976321	-1,256.76145511	-2,313.75848285	-2,217.43842302
E <sub>HOMO</sub> , eV	-4.64634638	-5.4417356	-6.05834587	-9.87937052
E <sub>LUMO</sub> , eV	-2.41038572	-1.7349988	-1.75186987	-8.78166269
ΔE, eV	2.23596066	3.706737	4.306476	1.097708
I = - E <sub>HOMO</sub> , eV	4.64634638	5.4417356	6.058346	9.87937052
A = - E <sub>LUMO</sub> , eV	2.41038572	1.7349988	1.75187	8.78166269
χ, eV	3.156018004	1.936132727	1.813597879	17.00000009
η, eV	1.11798033	1.853368385	2.153238	0.548853915
S, eV <sup>-1</sup>	0.44723506	0.26977907	0.232208423	0.91098922
μ, eV	-3.52836605	-3.588367185	-3.90510787	-9.330516605
Dipole Moment (Debye)	10.5480	14.6557	2.3535	8.0239

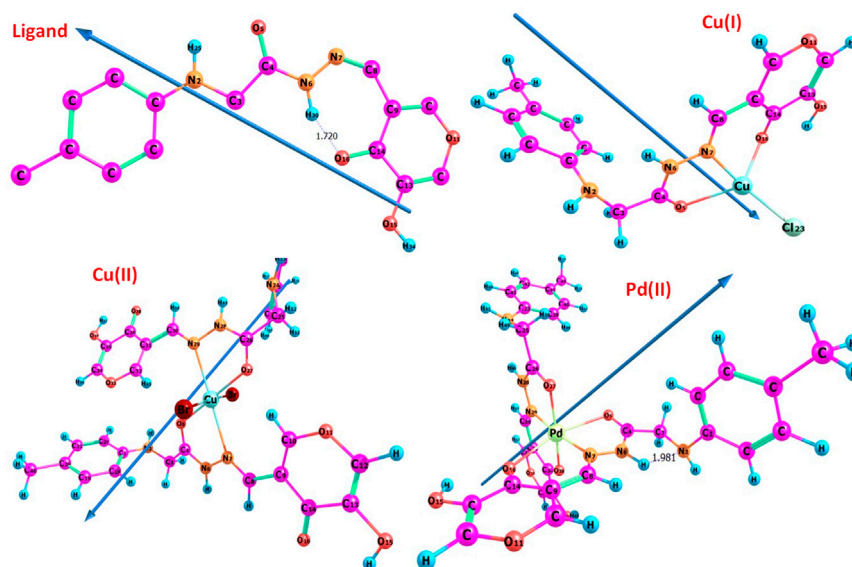


FIGURE 3  
Optimized geometry of all compounds.

respectively were changed to a higher frequency, while the bands of  $\nu(\text{C}=\text{O})_{\text{ring}}$  and  $\nu(\text{C}=\text{N})$  were changed to a lower frequency. New signals were seen in the region at 603, 600; 537, 536; and 537, 579  $\text{cm}^{-1}$  related to  $\nu$  (M-Oxygen) and  $\nu$  (M-Nitrogen) were seen in the region at 539, 545; 485, 479; and 508, 513  $\text{cm}^{-1}$  respectively (Elganzory et al., 2022). The infrared spectra for irradiated  $\text{H}_2\text{L}$  and chelates revealed changes in the size and intensity of the bands with the action of irradiation in all compounds (Abdalla et al., 2021). Supplementary Figure S7 shows the theoretical FT-IR spectra powder pattern of ligand and its complexes.

### 3.4 Mass spectra

$\text{Pd}(\text{H}_2\text{L})_2\text{Cl}_2 \cdot 2\text{H}_2\text{O}$ ,  $\text{Cu}(\text{H}_2\text{L})_2\text{Br}_2$ , and  $\text{Cu}(\text{H}_2\text{L})\text{Cl}$  showed molecular ion peaks at  $m/z$  815.11 (21%), 825.42 (12%), and 399.62 (32%). These findings were supported by the proposed molecular formulae that have been provided (calc. 815.95, 825.96, and 400.30 amu), respectively (Supplementary Figures S8-S10).

The mass fragmentation patterns of complexes are shown in Scheme S1-S3, where the mass spectra's multi-peaks pattern resulted in a sequence of peaks corresponding to the distinct fragments.

### 3.5 Electronic spectra

Table 3 and Supplementary Figures S11, S12 show all compounds' UV-Vis spectra before and after irradiation at room temperature in a  $10^{-3}$  DMF solution in the 200–800 nm range. In the UV range, the absorption spectra of  $\text{H}_2\text{L}_\text{B}$  and  $\text{H}_2\text{L}_\text{A}$  showed two absorption bands (Liu et al., 2013); the first bands were seen at  $\lambda_{\text{max}} = 341, 335$  nm related to  $\pi-\pi^*$  transition, and the second transitions were seen at  $\lambda_{\text{max}} = 399, 394$  nm assigned to  $n-\pi^*$  transition. The Pd(II) chelates ( $\text{B}_1$  and  $\text{A}_1$ ) explored bands at

332; 326, 393; 389 and 511; 502 nm, assigned to  $^1\text{A}_{1g} \rightarrow ^1\text{B}_{1g}$  transition representing a square planar geometry (El-Boraey and El-Gammal, 2015; Shankarwar et al., 2015). The electronic spectra of Cu(II) complexes ( $\text{B}_2$  and  $\text{A}_2$ ) revealed bands at 352, 346; 399, 394; and 571, 563 nm, pointing to  $n-\pi^*$  and d-d transition representing octahedral geometry. Moreover, Cu(I) chelates ( $\text{B}_3$  and  $\text{A}_3$ ) before and after irradiation revealed four bands at 343, 331; 399, 397; 487, 469; and 615, 595 nm, respectively, pointing to  $n-\pi^*$  and d-d transition representing tetrahedral geometry. The difference between the electronic transitions of the  $\text{H}_2\text{L}$  and all chelates was noted after irradiation as the  $\lambda_{\text{max}}$  position and the absorbance value (Abdalla et al., 2021).

### 3.6 X-ray diffraction

PXRD was used when the single crystals of the produced chelates failed to grow. Before and after irradiation, powder diffraction patterns of ligands ( $\text{H}_2\text{L}_\text{B}$ ,  $\text{H}_2\text{L}_\text{A}$ ) and Cu(II) complexes ( $\text{B}_2$ ) and ( $\text{A}_2$ ) were recorded across  $2\theta = 5^\circ-80^\circ$  (Table 4; Figure 1, Supplementary Figure S13). The greatest intensity peak was also identified, along with its location, half-maximum width, and  $d$  spacing. The reflection in the  $\text{H}_2\text{L}$  diffractogram peaks was shown at  $2\theta = 15.822^\circ$  and  $15.801^\circ$ , which corresponded to  $d$  values of 0.559119 and 0.558271 nm, respectively. Coordination compounds have been generated because the powder XRD patterns of the ligands ( $\text{H}_2\text{L}_\text{B}$ ,  $\text{H}_2\text{L}_\text{A}$ ) and the complexes ( $\text{B}_2$  and  $\text{A}_2$ ) were completely different. The patterns exhibited well-characterized crystalline peaks, indicating that the ligand was in crystallized form in the ( $\text{B}_2$  and  $\text{A}_2$ ) and ( $\text{H}_2\text{L}_\text{B}$ ,  $\text{H}_2\text{L}_\text{A}$ ) complexes. The average particle sizes of ( $\text{H}_2\text{L}_\text{B}$ ,  $\text{H}_2\text{L}_\text{A}$ ) and ( $\text{B}_2$  and  $\text{A}_2$ ) chelates were calculated using the Scherrer equation (Muniz et al., 2016; Abdalla et al., 2020; Abdel Rahman et al., 2022; Abdel-Rahman et al., 2022) and were

TABLE 7 Several bond lengths, Å and bond angles, degrees, for H<sub>2</sub>L and its metal chelates.

Bond length (Å)	H <sub>2</sub> L <sub>B</sub>	Cu(I) complex	Cu(II) complex	Pd(II) complex
R(C3-C4)	1.52898	1.53384	1.54370	1.53908
R(C4-O5)	1.24188	1.25226	1.26037	1.25313
R(C4-N6)	1.38249	1.38460	1.36856	1.38569
R(N6-N7)	1.36156	1.38528	1.39872	1.39448
R(N7-C8)	1.29829	1.31158	1.30142	1.31484
R(C8-C9)	1.48124	1.46039	1.46045	1.45667
R(C9-C14)	1.47007	1.46633	1.46249	1.46384
R(C14-O16)	1.26148	1.27469	1.27521	1.27649
R(H-N6)	1.03165	1.02151	1.01990	1.03504
R(O16-M)	---	2.26158	---	2.61590
R(N7-M)	---	2.06972	2.54149	2.07748
R(O5-M)	---	2.42471	2.03551	2.69381
R(X-M)	---	2.22424	2.53713	
Bond angles, degrees				
A(O16-C14-C9)	124.823	125.850	125.321	126.073
A(C14-C9-C8)	127.301	122.699	116.356	127.037
A(C9-C8-N7)	136.152	122.535	124.071	130.569
A(C8-N7-N6)	123.820	117.748	115.942	115.769
A(N7-N6-C4)	119.717	118.628	120.555	125.434
A(N6-C4-O5)	125.039	122.475	122.740	124.934
A(N6-C4-C3)	112.721	114.679	114.841	111.429
A(C4-C3-N2)	108.710	114.081	115.926	112.370
A(H-N6-N7)	118.934	123.115	119.567	121.790
A(O16-M-N7)	---	82.054	---	83.561
A(O5-M-N7)	---	74.188	73.428	74.038
A(C14-O16-M)	---	116.166	---	119.855
A(C8-N7-M)	---	127.184	143.087	129.815
A(Br-Cu-Br)	---	---	176.376	---
A(Cl-Cu-O5)	---	116.443	---	---
A(Cl-Cu-O16)	---	108.623	---	---

37.48; 31.99 and 51.64; 40.25 nm, respectively. The crystal size variation might be due to the Nano range caused by the irradiation.

### 3.7 Thermal studies

The thermal TGA of all compounds before (H<sub>2</sub>L<sub>B</sub>, B<sub>1</sub>-B<sub>3</sub>) and after (H<sub>2</sub>L<sub>A</sub>, A<sub>1</sub>-A<sub>3</sub>) irradiation were investigated with a heating range from (20°C–800°C). Table 5 and Supplementary Figure S14.

#### 3.7.1 Pd(II) chelates under the two irradiated and unirradiated cases

The TGA curves of chelates (B<sub>1</sub> and A<sub>1</sub>) (Supplementary Figure S14) showed three steps for losing weight (Calc./Exp.%: 13.35/13.27 and 13.35/13.32), assigned to the release of two hydrated water molecules and two hydrogen chloride molecules within the heat at 45–225°C. The second step showed the appearance of the decomposition within the heat from 225 to 386°C with losing weight (Calc/Exp.%: 71.64/71.59 and 71.64/71.61) and corresponded to C<sub>30</sub>H<sub>28</sub>N<sub>6</sub>O<sub>7</sub> leaving PdO as a residue (Aly and El-Boraey, 2019).



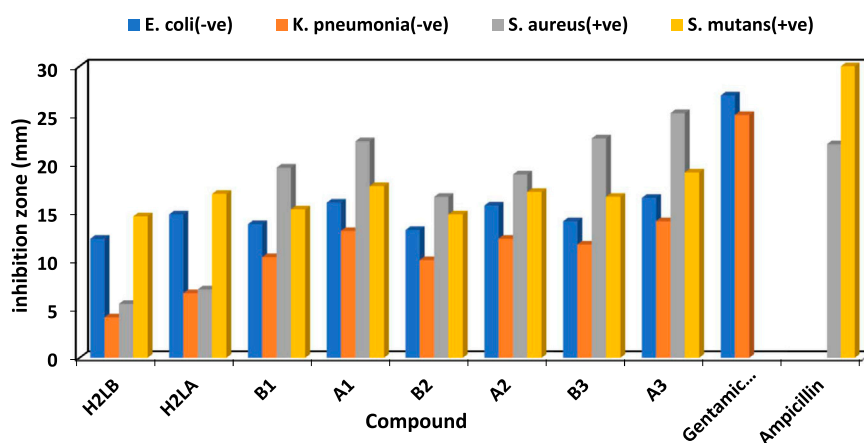


FIGURE 4 Antibacterial results (*In vitro*) of H<sub>2</sub>L and chelates before (B) and after (A) irradiation

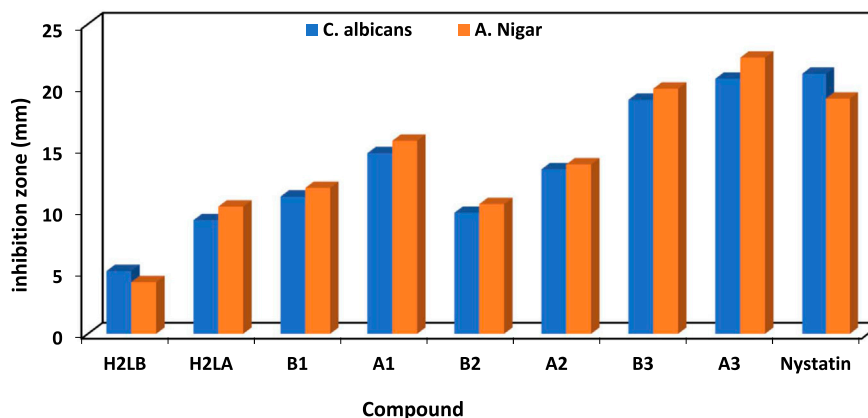


FIGURE 5 *In vitro* antifungal results of H<sub>2</sub>L and its chelates before (B) and after (A) irradiation.

TABLE 8 Topoisomerase IIa enzyme (code: 2xct) interaction with all compounds.

Docking 2xct			
Compound	Scoring energy (RMSD)	Active amino acids	Interaction type
H <sub>2</sub> L <sub>B</sub>	-3.7278(1.22)	Asp-512	Sidechain acceptor
Cu(I)	-7.2839(2.39)	Asp-508 and His1081	Side chain acceptor and Sidechain donor
Cu(II)	-4.1185(2.34)	---	Solvent contact
Pd(II)	-6.6027(2.34)	---	Solvent contact

### 3.7.2 Cu(II) chelates under the two irradiated and unirradiated cases

The TGA curves of the chelates (B<sub>2</sub> and A<sub>2</sub>) were four steps apart (Supplementary Figure S14), where weight loss was shown in the temperature ranges of 30–210 and 30–191°C (Calc./Found percent: 19.59/19.53 and 9.79/9.76) which agreed to the loss of two and one molecules of hydrogen bromide. The decomposition of (B<sub>2</sub> and A<sub>2</sub>) was within the heating range

210–305 and 191°C–461°C with weight loss (Calc./Exp.%: 23.03/23.13 and Calc./Found%: 34.88/34.91), which corresponded to the dissociation of C<sub>10</sub>H<sub>12</sub>N<sub>3</sub>O and C<sub>10</sub>H<sub>14</sub>N<sub>3</sub>O<sub>2</sub>Br. The third step in the range 305–591 and 461°C–610 °C indicated the removal of C<sub>20</sub>H<sub>16</sub>N<sub>3</sub>O<sub>6</sub> and C<sub>20</sub>H<sub>14</sub>N<sub>3</sub>O<sub>6</sub> with weight loss (Calc./Found%: 47.74/47.71 and 47.50/47.53). The final step over 591°C and 610 °C indicated the removal of CuO and Cu as the final remainder from unirradiated (B<sub>2</sub>) and irradiated

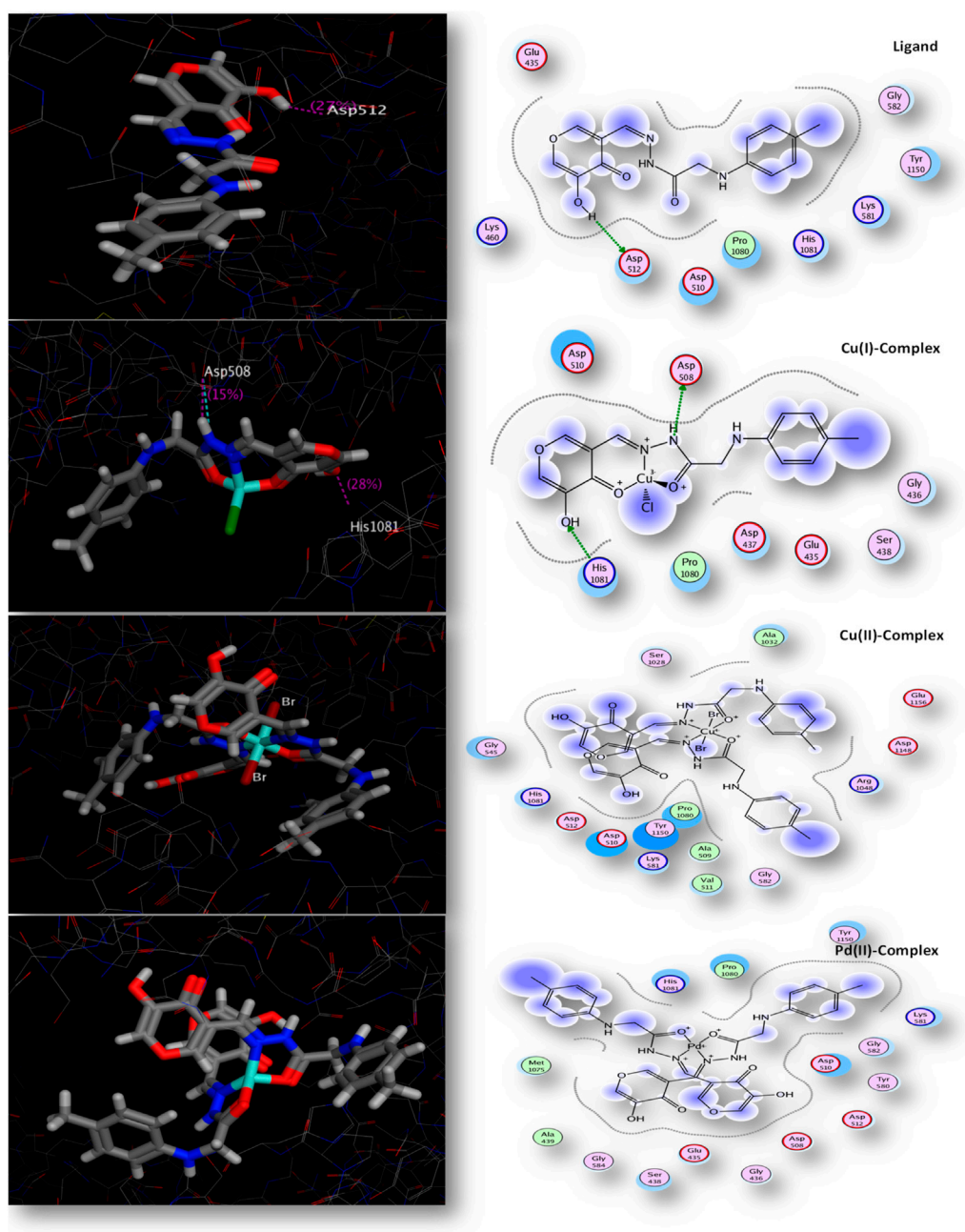


FIGURE 6  
2D and 3D interaction ability of all compounds with topoisomerase IIa enzyme (code: 2Xct).

Cu(II) complexes ( $A_2$ ), respectively (El-Boraey and Mansour, 2018).

### 3.7.3 Cu(I) chelates under the two irradiated and unirradiated cases

The TGA curves of chelates ( $B_3$  and  $A_3$ ) (Supplementary Figure S14) showed similar four steps within the heat range 100–19°C, which estimated the loss of hydrogen chloride molecule with mass loss (Calc./Found%: 9.12/9.09). The second step showed the mass loss (Calc./Found%: 38.25/38.21) in a temperature range of 198–495°C, corresponding to the losses of  $C_6H_5N_2O_3$ . The decomposition stage of ( $B_3$  and  $A_3$ ) through temperature range

495–571°C providing mass loss (Calc./Exp.%: 36.76/36.83) indicated the removal of  $C_9H_9NO$ , leaving copper metal as final residue. Finally, the thermal stability of the irradiated complexes using gamma rays was more thermally stable than the unirradiated complexes (Abdalla et al., 2021).

## 3.8 Molecular structure

When doing quantum chemistry research, the LUMO (p acceptor) and HOMO (p donor) molecular structures of  $H_2LB$  are important considerations. Frontier molecular orbitals (FMOs)

are the name given to these molecular orbitals. In HOMO and LUMO (Figure 2), the molecular structures of H<sub>2</sub>L<sub>B</sub> and its complexes were shown. The energies (E<sub>HOMO</sub>, E<sub>LUMO</sub>) of H<sub>2</sub>L<sub>B</sub> and its complexes are tabulated in Table 6. Both the E<sub>HOMO</sub> and E<sub>LUMO</sub> had negative values, indicating the stability. ( $\Delta E = E_{LUMO} - E_{HOMO}$ ) was the energy band gap that related to the charge transfer interface within the LUMO-HOMO of the molecule as specified in Table 6. The equations for dipole moment (D), hardness ( $\eta$ ), softness ( $\sigma$ ), chemical potential ( $\mu$ ), and electronegativity ( $\chi$ ) have been obtained and the corresponding results are shown in Table 6.

$$\eta = (I - A) / 2S = 1/2\eta \quad \mu = -(I + A)/2 \quad \chi = (I + A)/2\eta$$

$$I = -E_{HOMO} \quad A = -E_{LUMO}$$

Where I = the ionization potential of the molecule.

A = electron affinity of the molecule.

Hardness and softness, frequently used as chemical reactivity and stability indicators, were crucial parameters.

The molecule had a narrow gap between the HOMO and LUMO orbitals and became more reactive and softer, as smaller hardness ratings suggested higher reactivity. The order of softness was Pd > Ligand > Cu(I) > Cu(II). Except for the Pd(II) complex, every complex had a greater energy gap than the ligand. Therefore, the stability of most complexes under investigation was higher than the free ligand. The greater reactivity of the Pd(II) complex may be explained by the higher polarizability of the second-row transition elements (Palladium) in comparison to the first-row elements (Copper).

The atom ordering of H<sub>2</sub>L<sub>B</sub> was given in the molecular structure, and complexes were also presented (Figure 3). The following observations were based on the calculated bond lengths and orientations directed at the compounds (Table 7).

In the complexes some bond lengths were increased [(C3-C4), (N7-C8), (C14-O16), (N6-N7) and (C4-O5)] and others were decreased [(C8-C9) and (C9-C14)] to adjust the coordination via the N7, O5, and O16-atoms in both Cu(I) and Pd(II) complexes with the emergence of new O16-M, (N7-M), and (O5-M) bonds. In the case of the Cu(II) complex, the coordination was carried out through N7 and O5 atoms comp, leaving the coordination sphere via bromide bonding. As seen in Table 7, coordination modified the H<sub>2</sub>L<sub>B</sub> bond angles, and when the metal center was changed, significant changes in the angles surrounding the metal also occurred. The significant swing in angle values due to bonding during complex formation was either increased or decreased. N7, O5, and O16 atoms in the ligand calculated natural charges of -0.197, -0.583, and -0.589 respectively as seen in Supplementary Table S1. Charge transfer from L(ligand) → M(metal) could be supported by decreased calculated charges on metal ions after coordination (Hassan and Gomha, 2019). The charges changed from Cu(I), Cu(II), and Pd(II) to 0.503, 0.0255, and 0.488 respectively. The theoretical results of FTIR showed good agreement with the experimental results as seen in Table 2 and Supplementary Figures S3-S6. The theoretical infrared spectra of the ligand L showed noteworthy absorption regions at 344, 1700, 1,633, and 1,597 cm<sup>-1</sup> corresponding to ν N-H), (C=O) side, (C=O) ring, and (C=N) vibrations. However, when these vibrations were complexed with metal ions, their positions shifted from their initial values. Also, the electronic transitions of

ligands and complexes in the presence of solvent effect were calculated and the transition values are tabulated in Table 3.

### 3.9 Antimicrobial study

The antibacterial properties of the H<sub>2</sub>L and its chelates were tested against different Gram-positive and negative strains of bacteria both before and after exposure to gamma irradiation. Additionally, it had antifungal effects against *Candida albicans* and *Aspergillus Nigar*. The conventional antimicrobial agents used for antibacterial and antifungal research purposes included ampicillin, gentamicin, and nystatin.

The efficacy of the antibacterial properties of all produced compounds is demonstrated in Supplementary Table S2 and Figure 4 and Figure 5. The findings suggested that complexes exhibited more activity compared to ligands. Furthermore, following irradiation, complexes demonstrated enhanced efficacy as antibacterial and antifungal agents, surpassing their pre-irradiation performance (Aly and Elembaby, 2020a; Abdalla et al., 2021). The increased activity of complexes may be elucidated by Overton's notion (Anjaneyulu and Rao, 1986), as evidenced in our prior studies (Khalf-Alla et al., 2019; Hassan and Khalf-Alla, 2020; Hassan and Mohamed, 2020). The reduction in polarity of the metal ion occurred as a result of chelation, due to the interaction between its partial positive charge and the donation sites of the coordinated ligand. Additionally, chelation promoted the dispersion of π-electrons throughout the whole chelate ring, hence enhancing the lipophilic nature of the chemical under investigation. The compound's lipophilic nature facilitated its penetration through the lipid layer of the cell membrane, resulting in a more potent and destructive effect on the cells. Moreover, the Cu(I) complex exhibited enhanced antibacterial activity after irradiation (A<sub>3</sub>), surpassing the antibacterial activity of the Cu(I) complex before irradiation (B<sub>3</sub>) against bacterial species compared to other substances, including standard drugs like ampicillin and gentamicin. Similarly, when nystatin was used as a standard drug, the Cu(I) complex also displayed superior antifungal activity.

### 3.10 Evaluation of docking studies

A nitrogen-containing heterocyclic molecule is an essential scaffold with antibacterial potential. Therefore, our research aimed to synthesize and investigate new nitrogen-containing heterocyclic compounds experimentally *in vitro* against different bacterial strains and theoretically using MOE 2008 software (Hassan and Mohamed, 2020). A molecular docking study was performed with the target site of topoisomerase enzyme(2xt) chain a from the protein data bank. The topoisomerase enzyme is a crucial enzyme that plays a vital role in the process of DNA replication (Redgrave et al., 2014). The gyrase enzyme facilitates the relaxing of super-coiled DNA during DNA replication by breaking and rejoining both strands of the DNA chain, allowing for unwinding and replication (Champoux, 2001).

There was a good correlation between the *in vitro* antimicrobial inhibition assay and the scoring energy values, as shown in Table 8 and Supplementary Table S3. The Palladium (II) and Copper (I) complexes revealed effective results against most microbes. The

explored binding affinity was the best-posed interaction with low root mean square deviation values (RMSD). Figure 6 displays the different binding interaction types of compounds with 2xct protein. The Copper(I) complex showed sidechain acceptor and sidechain donor interaction types with Asp-508 and His1081 amino acid residues, respectively. The reactivity sequence relative to the scoring energy values was Cu(I) > Pd(II) > Cu(II) > L, which showed good fitting with the zone inhibition values experimentally where the Cu(I) complex inhibited bacterial growth in both Gram-positive and Gram-negative bacteria, with zone inhibition values that were greater than those of the Pd(II), Cu(II), and ligand compounds. The binding affinity of our compounds consistently demonstrated superior or equivalent values in multiple prior studies targeting the same protein type (Pisano et al., 2019; El-Etrawy and Sherbiny, 2021). Paraphrased, (Several compounds were examined before against the same 2xct protein and observed high affinity to inhibit the examined protein with scoring energies  $-9.41$  relative to Cu(II) chelate (Aly et al., 2023). Our new Cu(I) chelate observed a similar affinity to the 2xct protein in the present paper. Also, our compounds achieved a 2xct protein inhibition effect in the docking scoring range ( $-3.63$  to  $-8.51$ ) observed for the quinolone moiety-based compounds (Patel and Patel, 2014).

## 4 Conclusion

Based on a novel ( $H_2L_B$ ) ligand (Z)-2-(phenylamino)-N'-(thiophen-2-ylmethylene) acetohydrazide, three new chelates, Pd(II), Cu(II), and Cu(I), have been isolated. Based on the outcomes of various characterization approaches, the hypothesized structures of the ( $H_2L_B$ ) and its chelates verified the production of 1:2 Pd(II) and Cu(II) and 1:1 (M:L) Cu(I) chelates. The molar conductance values of the chelates demonstrated their non-electrolytic character except for the ionic Pd(II) Complex. The effectiveness of the antibacterial and antifungal treatments was compared to the industry-standard medications ampicillin, gentamicin, and nystatin. Paraphrased, (Zone inhibition values revealed that the Cu(I) complex after irradiation (A3) acquired better antibacterial activity followed by the Cu(I) complex before irradiation (B3) relative to bacterial species than others, when ampicillin and gentamicin as reference drugs, as well as the antifungal species when nystatin was used as a standard drug). The antimicrobial activity of these complexes followed the order: Cu(I) complex > Pd(II) complex > Cu(II) complex > Ligand. The geometries of the Pd(II) complex were square planar, according to the DFT calculations performed on the synthesized compounds. Cu(II) was octahedral, with hex coordinates chosen around the metal ions, while Cu(I) complex had a tetrahedral geometry. The synthesized ligand and the range of antibacterial activity of all the metal complexes against bacterial species were satisfactory. The docking stimulation revealed all of the chemicals' binding models.

## References

Abdalla, E. M., Abdel Rahman, L. H., Abdelhamid, A. A., Shehata, M. R., Alothman, A. A., and Nafady, A. (2020). Synthesis, characterization, theoretical studies, and antimicrobial/antitumor potencies of salen and salen/imidazole complexes of Co (II), Ni (II), Cu (II), Cd (II), Al (III) and La (III). *Appl. Organomet. Chem.* 34, e5912. doi:10.1002/aoc.5912

## Data availability statement

The original contributions presented in the study are included in the article/Supplementary Material, further inquiries can be directed to the corresponding authors.

## Author contributions

SH: Data curation, Formal Analysis, Investigation, Methodology, Software, Writing—original draft. SA: Conceptualization, Data curation, Methodology, Supervision, Visualization, Writing—review and editing. AA-S: Data curation, Formal Analysis, Investigation, Resources, Validation, Writing—review and editing. SA: Data curation, Formal Analysis, Resources, Writing—original draft. MS: Conceptualization, Data curation, Formal Analysis, Investigation, Resources, Writing—review and editing. GN: Data curation, Formal Analysis, Investigation, Resources, Writing—review and editing. EA: Conceptualization, Data curation, Formal Analysis, Investigation, Methodology, Validation, Visualization, Writing—original draft, Writing—review and editing.

## Funding

The author(s) declare that no financial support was received for the research, authorship, and/or publication of this article.

## Conflict of interest

The authors declare that the research was conducted in the absence of any commercial or financial relationships that could be construed as a potential conflict of interest.

## Publisher's note

All claims expressed in this article are solely those of the authors and do not necessarily represent those of their affiliated organizations, or those of the publisher, the editors and the reviewers. Any product that may be evaluated in this article, or claim that may be made by its manufacturer, is not guaranteed or endorsed by the publisher.

## Supplementary material

The Supplementary Material for this article can be found online at: <https://www.frontiersin.org/articles/10.3389/fchem.2024.1357330/full#supplementary-material>

Abdalla, E. M., Hassan, S. S., Elganzory, H. H., Aly, S. A., and Alshater, H. (2021). Molecular docking, DFT calculations, effect of high energetic ionizing radiation, and biological evaluation of some novel metal (II) heteroleptic complexes bearing the thiosemicarbazone ligand. *Molecules* 26, 5851. doi:10.3390/molecules26195851

- Abdrazzaq, E., Jbarah, A. A., Al-Noor, T. H., Shinain, G. T., and Jawad, M. M. (2022). Synthesis, DFT calculations, DNA interaction, and antimicrobial studies of some mixed ligand complexes of oxalic acid and Schiff base trimethoprim with various metal ions. *Indonesian J. Chem.* 22, 1348–1364. doi:10.22146/ijc.74020
- Abdel Rahman, L. H., Al-Zaqri, N., Abdelghani, A. A., and Abdalla, E. M. (2022). Physicochemical, *in vitro* therapeutic activity, DNA-binding, and *in silico* molecular docking studies of samarium (III) complexes bearing N, O-chelated Schiff base ligands. *J. Coord. Chem.* 75, 994–1018. doi:10.1080/00958972.2022.2095267
- Abdel-Rahman, L. H., Basha, M. T., Al-Farhan, B. S., Shehata, M. R., and Abdalla, E. M. (2022). Synthesis, characterization, potential antimicrobial, antioxidant, anticancer, DNA binding, and molecular docking activities and DFT on novel Co (II), Ni (II), VO (II), Cr (III), and La (III) Schiff base complexes. *Appl. Organomet. Chem.* 36, e6484. doi:10.1002/aoc.6484
- Aghatabay, N. M., Somer, M., Senel, M., Dulger, B., and Guçin, F. (2007). Raman, FT-IR, NMR spectroscopic data and antimicrobial activity of bis[μ<sub>2</sub>-(benzimidazol-2-yl)-2-ethanethiolato-N,S,S'-chloro-palladium(II)] dimer, [(μ<sub>2</sub>-CH<sub>2</sub>CH<sub>2</sub>NHCC6H<sub>4</sub>)PdCl] 2·C<sub>2</sub>H<sub>5</sub>OH complex. *Eur. J. Med. Chem.* 42, 1069–1075. doi:10.1016/j.ejmech.2007.01.011
- Al-Farhan, B. S., Basha, M. T., Abdel Rahman, L. H., El-Saghier, A. M., El-Ezz, A., Marzouk, A. A., et al. (2021). Synthesis, dft calculations, antiproliferative, bactericidal activity and molecular docking of novel mixed-ligand salen/8-hydroxyquinoline metal complexes. *Molecules* 26, 4725. doi:10.3390/molecules26164725
- Al-Hazmi, G. A., Abou-Melha, K. S., El-Metwaly, N. M., Althagafi, I., Shaaban, F., Elghalban, M. G., et al. (2020). Spectroscopic and theoretical studies on Cr (III), Mn (II) and Cu (II) complexes of hydrazone derived from picolinic hydrazide and O-vanillin and evaluation of biological potency. *Appl. Organomet. Chem.* 34, e5408. doi:10.1002/aoc.5408
- Anjaneyulu, Y., and Rao, R. P. (1986). Preparation, characterization and antimicrobial activity studies on some ternary complexes of Cu (II) with acetylacetone and various salicylic acids. *Synth. React. Inorg. Met.-Org. Chem.* 16 (2), 257–272.
- Alodeani, E. A., Arshad, M., and Izhari, M. A. (2015). Anti-uropathogenic activity, drug likeness, physicochemical and molecular docking assessment of (E)-N'-(substituted-benzylidene)-2-(quinolin-8-yloxy) acetohydrazide. *Asian Pac. J. Trop. Biomed.* 5, 676–683. doi:10.1016/j.apjtb.2015.04.010
- Aly, S., and El-Boraey, H. A. (2019). Effect of gamma irradiation on spectral, XRD, SEM, DNA binding, molecular modeling and antibacterial property of some (Z) N-(furan-2-yl) methylene)-2-(phenylamino) acetohydrazide metal (II) complexes. *J. Mol. Struct.* 1185, 323–332. doi:10.1016/j.molstruc.2019.02.069
- Aly, S., and Elembaby, D. (2020a). Synthesis, spectroscopic characterization and study the effect of gamma irradiation on VO<sub>2</sub><sup>+</sup>, Mn<sup>2+</sup>, Zn<sup>2+</sup>, Ru<sup>3+</sup>, Pd<sup>2+</sup>, Ag<sup>+</sup> and Hg<sup>2+</sup> complexes and antibacterial activities. *Arab. J. Chem.* 13, 4425–4447. doi:10.1016/j.arabjc.2019.08.007
- Aly, S., and Elembaby, D. (2020b). Synthesis, spectroscopic characterization and study the effect of gamma irradiation on VO<sub>2</sub><sup>+</sup>, Mn<sup>2+</sup>, Zn<sup>2+</sup>, Ru<sup>3+</sup>, Pd<sup>2+</sup>, Ag<sup>+</sup> and Hg<sup>2+</sup> complexes and antibacterial activities. *Arabian J. Chem.* 13, 4425–4447. doi:10.1016/j.arabjc.2019.08.007
- Aly, S., and Fathalla, S. (2020). Preparation, characterization of some transition metal complexes of hydrazone derivatives and their antibacterial and antioxidant activities. *Arabian J. Chem.* 13, 3735–3750. doi:10.1016/j.arabjc.2019.12.003
- Aly, S. A., Elganzory, H. H., Mahross, M. H., and Abdalla, E. M. (2021). Quantum chemical studies and effect of gamma irradiation on the spectral, thermal, X-ray diffraction and DNA interaction with Pd (II), Cu (I), and Cd (II) of hydrazone derivatives. *Appl. Organomet. Chem.* 35, e6153. doi:10.1002/aoc.6153
- Aly, S. A., Hassan, S. S., El-Boraey, H. A., Eldourghamy, A., Abdalla, E. M., Alminderej, F. M., et al. (2023). Synthesis, biological activity, and the effect of ionization radiation on the spectral, XRD, and TGA analysis of Cu (I), Cu (II), Zn (II), and Cd (II) complexes. *Arabian J. Sci. Eng.* 49, 361–379. doi:10.1007/s13369-023-07988-2
- Aly, S. A., Hassan, S. S., Eldourghamy, A. S., Badr, E. E., El-Salamoney, M. A., Hassan, M. A., et al. (2022a). Synthesis, characterization, XRD, SEM, DNA binding and effect of γ-irradiation of some new Ni (II) and Co (II) complexes with thiosemicarbazone ligand. *in vitro* antimicrobial and antioxidant activities. *Appl. Organomet. Chem.* 36, e6727. doi:10.1002/aoc.6727
- Aly, S. A., Hassan, S. S., Eldourghamy, A. S., Badr, E. E., El-Salamoney, M. A., Hassan, M. A., et al. (2022b). Synthesis, characterization, XRD, SEM, DNA binding, and effect of γ-irradiation of some new Ni (II) and Co (II) complexes with thiosemicarbazone ligand: *in vitro* antimicrobial and antioxidant activities. *Appl. Organomet. Chem.* 36, e6727. doi:10.1002/aoc.6727
- Ammar, R. A., Alaghaz, A.-N. M., and Elhenawy, A. A. (2014). DFT, characterization and investigation of vibrational spectroscopy of 4-(4-hydroxy)-3-(2-pyrazine-2-carbonyl) hydrazonemethylphenyl-diazen-yl-benzenesulfonamide and its copper (II) complex. *J. Mol. Struct.* 1067, 94–103. doi:10.1016/j.molstruc.2014.02.051
- Anastassova, N. O., Yancheva, D. Y., Mavrova, A. T., Kondeva-Burdina, M. S., Tzankova, V. I., Hristova-Avakumova, N. G., et al. (2018). Design, synthesis, antioxidant properties and mechanism of action of new N, N'-disubstituted benzimidazole-2-thione hydrazone derivatives. *J. Mol. Struct.* 1165, 162–176. doi:10.1016/j.molstruc.2018.03.119
- Aneja, B., Khan, N. S., Khan, P., Queen, A., Hussain, A., Rehman, M. T., et al. (2019). Design and development of Isatin-triazole hydrazones as potential inhibitors of microtubule affinity-regulating kinase 4 for the therapeutic management of cell proliferation and metastasis. *Eur. J. Med. Chem.* 163, 840–852. doi:10.1016/j.ejmech.2018.12.026
- Babahan, I., Özmen, A., Aksel, M., Bilgin, M. D., Gumusada, R., Gunay, M. E., et al. (2020). A novel bidentate ligand containing oxime, hydrazone and indole moieties and its BF<sub>2</sub><sup>+</sup> bridged transition metal complexes and their efficiency against prostate and breast cancer cells. *Appl. Organomet. Chem.* 34, e5632. doi:10.1002/aoc.5632
- Balashova, T. V., Obolensky, S. V., Trufanov, A. N., Ivin, M. N., Ilichev, V. A., Kukinov, A. A., et al. (2019). Impact of n, γ-irradiation on organic complexes of rare earth metals. *Sci. Rep.* 9, 13314–13316. doi:10.1038/s41598-019-49962-9
- Beeton, M. L., Aldrich-Wright, J. R., and Bolhuis, A. (2014). The antimicrobial and antibiofilm activities of copper (II) complexes. *J. Inorg. Biochem.* 140, 167–172. doi:10.1016/j.jinorgbio.2014.07.012
- Bergamini, F. R., Nunes, J. H., De Carvalho, M. A., Ribeiro, M. A., De Paiva, P. P., Banzato, T. P., et al. (2019). Polynuclear copper (II) complexes with nalidixic acid hydrazones: antiproliferative activity and selectivity assessment over a panel of tumor cells. *Inorganica Chim. Acta* 484, 491–502. doi:10.1016/j.ica.2018.09.084
- Biyala, M. K., Sharma, K., Swami, M., Fahmi, N., and Singh, R. V. (2008). Spectral and biocidal studies of palladium (II) and platinum (II) complexes with monobasic bidentate Schiff bases. *Transit. Metal. Chem.* 33, 377–381. doi:10.1007/s11243-008-9053-3
- Cao, W., Liu, Y., Zhang, T., and Jia, J. (2018). Synthesis, characterization, theoretical and antimicrobial studies of tridentate hydrazone metal complexes of Zn (II), Cd (II), Cu (II) and Co (III). *Polyhedron* 147, 62–68. doi:10.1016/j.poly.2018.03.012
- Champoux, J. J. (2001). DNA topoisomerases: structure, function, and mechanism. *Annu. Rev. Biochem.* 70, 369–413. doi:10.1146/annurev.biochem.70.1.369
- Coimbra, E. S., De Souza, M. V. N., Terror, M. S., Pinheiro, A. C., and Da Trindade Granato, J. (2019). Synthesis, biological activity, and mechanism of action of new 2-pyrimidinyl hydrazone and N-acylhydrazone derivatives, a potent and new classes of antileishmanial agents. *Eur. J. Med. Chem.* 184, 111742. doi:10.1016/j.ejmech.2019.111742
- Dehestani, L., Ahangar, N., Hashemi, S. M., Irannejad, H., Masihi, P. H., Shakiba, A., et al. (2018). Design, synthesis, *in vivo* and *in silico* evaluation of phenacyl triazole hydrazones as new anticonvulsant agents. *Bioorg. Chem.* 78, 119–129. doi:10.1016/j.bioorg.2018.03.001
- Ding, C.-C., Wu, S.-Y., Xu, Y.-Q., Wu, L.-N., and Zhang, L.-J. (2018). DFT studies for three Cu (II) coordination polymers: geometrical and electronic structures, g factors and UV-visible spectra. *Chem. Phys.* 508, 20–25. doi:10.1016/j.chemphys.2018.04.016
- Dorotíková, S., Kožíšková, J., Malček, M., Jomová, K., Herich, P., Plevová, K., et al. (2015). Copper (II) complexes with new fluoroquinolones: synthesis, structure, spectroscopic and theoretical study, DNA damage, cytotoxicity and antiviral activity. *J. Inorg. Biochem.* 150, 160–173. doi:10.1016/j.jinorgbio.2015.06.017
- Ekennia, A. C., Osowole, A. A., Onwudiwe, D. C., Babahan, I., Ibeji, C. U., Okafor, S. N., et al. (2018). Synthesis, characterization, molecular docking, biological activity and density functional theory studies of novel 1, 4-naphthoquinone derivatives and Pd (II), Ni (II) and Co (II) complexes. *Appl. Organomet. Chem.* 32, e4310. doi:10.1002/aoc.4310
- El-Boraey, H. A., and El-Gammal, O. A. (2015). New 15-membered tetraaza (N<sub>4</sub>) macrocyclic ligand and its transition metal complexes: spectral, magnetic, thermal and anticancer activity. *Spectrochimica Acta Part A Mol. Biomol. Spectrosc.* 138, 553–562. doi:10.1016/j.saa.2014.11.015
- El-Boraey, H. A., and Mansour, A. I. (2018). Synthesis, spectral and gamma ray irradiation studies on metal complexes of N, N'-naphthalene-1, 8-diyllbis (2-aminobenzamide). *Inorg. Nano-Metal Chem.* 48, 8–15. doi:10.1080/24701556.2017.1357588
- El-Etrawy, A.-a.S., and Sherbiny, F. F. (2021). Design, synthesis, biological assessment and molecular docking studies of some new 2-Thioxo-2, 3-dihydropyrimidin-4 (1H)-ones as potential anticancer and antibacterial agents. *J. Mol. Struct.* 1225, 129014. doi:10.1016/j.molstruc.2020.129014
- Elganzory, H. H., Hassan, S. S., Aly, S. A., and Abdalla, E. M. (2022). Synthesis, characterization, PXRD studies, theoretical calculation, and antitumor potency studies of a novel N, O-multidentate chelating ligand and its Zr (IV), V (IV), Ru (III), and Cd (II) complexes. *Bioinorg. Chem. Appl.* 2022, 1–20. doi:10.1155/2022/2006451
- El-Saied, F. A., Shakhdofa, M. M., Al-Hakimi, A. N., and Shakhdofa, A. M. (2020). Transition metal complexes derived from N'-(4-fluorobenzylidene)-2-(quinolin-2-yloxy) acetohydrazide: synthesis, structural characterization, and biocidal evaluation. *Appl. Organomet. Chem.* 34, e5898. doi:10.1002/aoc.5898
- Elsayed, S. A., El-Gharabawy, H. M., Butler, I. S., and Atlam, F. M. (2020). Novel metal complexes of 3-acetyl coumarin-2-hydrazinobenzothiazole Schiff base: design, structural characterizations, DNA binding, DFT calculations, molecular docking and biological studies. *Appl. Organomet. Chem.* 34, e5643. doi:10.1002/aoc.5643
- Frisch, A., Hratchian, H. P., Dennington Ii, R., Keith, T., Millam, J., Nielsen, B., et al. (2009a). *GaussView version 5.0*. 8. Wallingford, CT: Gaussian, Inc.
- Frisch, M., Trucks, G., Schlegel, H., Scuseria, G., Robb, M., Cheeseman, J., et al. (2009b). *Gaussian 09, revision A. 02*. Wallingford, CT: Gaussian, Inc.

- Garoufis, A., Hadjikakou, S., and Hadjiliadis, N. (2009). Palladium coordination compounds as anti-viral, anti-fungal, anti-microbial and anti-tumor agents. *Coord. Chem. Rev.* 253, 1384–1397. doi:10.1016/j.ccr.2008.09.011
- Guerra, W., De Andrade Azevedo, E., De Souza Monteiro, A. R., Bucciarelli-Rodriguez, M., Chartone-Souza, E., Nascimento, A. M. A., et al. (2005). Synthesis, characterization, and antibacterial activity of three palladium (II) complexes of tetracyclines. *J. Inorg. Biochem.* 99, 2348–2354. doi:10.1016/j.jinorgbio.2005.09.001
- Haghighijoo, Z., Firuzi, O., Hemmateenejad, B., Emami, S., Edraki, N., and Miri, R. (2017). Synthesis and biological evaluation of quinazolinone-based hydrazones with potential use in Alzheimer's disease. *Bioorg. Chem.* 74, 126–133. doi:10.1016/j.bioorg.2017.07.014
- Hassan, S. S., and Gomha, S. M. (2019). Novel functionalized thiosemicarbazone ligands and their Pd (II) complexes: synthesis, characterization, antibacterial and cytotoxic activities. *Chem. Pap.* 73, 331–344. doi:10.1007/s11696-018-0592-6
- Hassan, S. S., and Khalf-Alla, P. A. (2020). Anti-hepatocellular carcinoma, antioxidant, antiinflammation and antimicrobial investigation of some novel first and second transition metal complexes. *Appl. Organomet. Chem.* 34 (4), e5432.
- Hassan, S. S., and Mohamed, E. F. (2020). Antimicrobial, antioxidant and antitumor activities of Nano-Structure Eu (III) and La (III) complexes with nitrogen donor tridentate ligands. *Appl. Organomet. Chem.* 34, e5258. doi:10.1002/aoc.5258
- Hoonur, R. S., Patil, B. R., Badiger, D. S., Vadavi, R. S., Gudasi, K. B., Dandawate, P. R., et al. (2010). Transition metal complexes of 3-aryl-2-substituted 1, 2-dihydroquinazolin-4 (3H)-one derivatives: new class of analgesic and anti-inflammatory agents. *Eur. J. Med. Chem.* 45, 2277–2282. doi:10.1016/j.ejmech.2010.01.072
- Hubin, T. J., Amoyaw, P. N.-A., Roewe, K. D., Simpson, N. C., Maples, R. D., Freeman, T. N. C., et al. (2014). Synthesis and antimalarial activity of metal complexes of cross-bridged tetraazamacrocyclic ligands. *Bioorg. Med. Chem.* 22, 3239–3244. doi:10.1016/j.bmc.2014.05.003
- Katariya, K. D., Shah, S. R., and Reddy, D. (2020). Anticancer, antimicrobial activities of quinoline based hydrazone analogues: synthesis, characterization and molecular docking. *Bioorg. Chem.* 94, 103406. doi:10.1016/j.bioorg.2019.103406
- Khalf-Alla, P. A., Hassan, S. S., and Shoukry, M. M. (2019). Complex formation equilibria, DFT, docking, antioxidant and antimicrobial studies of iron (III) complexes involving Schiff bases derived from glucosamine or ethanolamine. *Inorganica Chim. Acta* 492, 192–197.
- Khan, S. A., Rizwan, K., Shahid, S., Noamaan, M. A., Rasheed, T., and Amjad, H. (2020). Synthesis, DFT, computational exploration of chemical reactivity, molecular docking studies of novel formazan metal complexes and their biological applications. *Appl. Organomet. Chem.* 34, e5444. doi:10.1002/aoc.5444
- Lemoine, P., Viostat, B., Morgant, G., Greenaway, F. T., Tomas, A., Dung, N.-H., et al. (2020). Synthesis, crystal structure, EPR properties, and anti-convulsant activities of binuclear and mononuclear 1, 10-phenanthroline and salicylate ternary copper (II) complexes. *J. Inorg. Biochem.* 89, 18–28. doi:10.1016/s0162-0134(01)00324-5
- Liu, Y.-T., Lian, G.-D., Yin, D.-W., and Su, B.-J. (2013). Synthesis, characterization and biological activity of ferrocene-based Schiff base ligands and their metal (II) complexes. *Spectrochimica Acta Part A Mol. Biomol. Spectrosc.* 100, 131–137. doi:10.1016/j.saa.2012.03.049
- Lobana, T. S., Indoria, S., Jassal, A. K., Kaur, H., Arora, D. S., and Jasinski, J. P. (2014). Synthesis, structures, spectroscopy and antimicrobial properties of complexes of copper (II) with salicylaldehyde N-substituted thiosemicarbazones and 2, 2'-bipyridine or 1, 10-phenanthroline. *Eur. J. Med. Chem.* 76, 145–154. doi:10.1016/j.ejmech.2014.02.009
- Mahani, N. M., and Mohammadi, S. Z. (2022). Studies of quantum mechanics/molecular docking on zanubrutinib as potential repurposed against Covid-19. *Bull. Chem. Soc. Ethiop.* 36, 479–485. doi:10.4314/bcse.v36i2.19
- Mandewale, M. C., Patil, U. C., Shedge, S. V., Dappadwad, U. R., and Yamgar, R. S. (2017). A review on quinoline hydrazone derivatives as a new class of potent antitubercular and anticancer agents. *Beni-Suef Univ. J. basic Appl. Sci.* 6, 354–361. doi:10.1016/j.bjbas.2017.07.005
- Mandewale, M. C., Thorat, B., Nivid, Y., Jadhav, R., Nagarsekar, A., and Yamgar, R. (2018). Synthesis, structural studies and antituberculosis evaluation of new hydrazone derivatives of quinoline and their Zn (II) complexes. *J. Saudi Chem. Soc.* 22, 218–228. doi:10.1016/j.jscs.2016.04.003
- Manohar, C. S., Manikandan, A., Sridhar, P., Sivakumar, A., Kumar, B. S., and Reddy, S. R. (2018). Drug repurposing of novel quinoline acetohydrazide derivatives as potent COX-2 inhibitors and anti-cancer agents. *J. Mol. Struct.* 1154, 437–444. doi:10.1016/j.molstruc.2017.10.075
- Margariti, A., Papakonstantinou, V. D., Stamatakis, G. M., Demopoulos, C. A., Schnakenburg, G., Andreopoulou, A. K., et al. (2020). Substituted pyridine-quinoline ligands as building blocks for neutral rhodium (III) complexes. Synthesis, structural characterization studies and anti-platelet activity towards the Platelet-Activating Factor (PAF). *Polyhedron* 178, 114336. doi:10.1016/j.poly.2019.114336
- Maurya, R., Malik, B., Mir, J., Vishwakarma, P., Rajak, D., and Jain, N. (2015). Nickel (II) complexes of ONS donor Schiff base ligands: synthesis, combined DFT-experimental characterization, redox, thermal, and *in vitro* biological investigation. *J. Coord. Chem.* 68, 2902–2922. doi:10.1080/00958972.2015.1064526
- Maurya, S. S., Khan, S. I., Bahuguna, A., Kumar, D., and Rawat, D. S. (2017). Synthesis, antimalarial activity, heme binding and docking studies of N-substituted 4-aminoquinoline-pyrimidine molecular hybrids. *Eur. J. Med. Chem.* 129, 175–185. doi:10.1016/j.ejmech.2017.02.024
- Meira, C. S., Dos Santos Filho, J. M., Sousa, C. C., Anjos, P. S., Cerqueira, J. V., Neto, H. A. D., et al. (2018). Structural design, synthesis and substituent effect of hydrazone-N-acylhydrazones reveal potent immunomodulatory agents. *Bioorg. Med. Chem.* 26, 1971–1985. doi:10.1016/j.bmc.2018.02.047
- Muniz, F. T. L., Miranda, M. a.R., Morilla Dos Santos, C., and Sasaki, J. M. (2016). The Scherrer equation and the dynamical theory of X-ray diffraction. *Acta Crystallogr. Sect. A Found. Adv.* 72, 385–390. doi:10.1107/s205327311600365x
- Naveen, P., Vijaya Pandiyan, B., Anu, D., Dallemer, F., Kolandaivel, P., and Prabhakaran, R. (2020). A pseudo trinuclear nickel-sodium complex containing tris (8-methyl-2-oxo-quinolidineamino ethylamine): synthesis, spectral characterization, X-ray crystallography and *in vitro* biological evaluations. *Appl. Organomet. Chem.* 34, e5605. doi:10.1002/aoc.5605
- Netalkar, P. P., Netalkar, S. P., Budagumpi, S., and Revankar, V. K. (2014). Synthesis, crystal structures and characterization of late first row transition metal complexes derived from benzothiazole core: anti-tuberculosis activity and special emphasis on DNA binding and cleavage property. *Eur. J. Med. Chem.* 79, 47–56. doi:10.1016/j.ejmech.2014.03.083
- Özbek, N., Özdemir, Ü. Ö., Altun, A. F., and Şahin, E. (2019). Sulfonamide-derived hydrazone compounds and their Pd (II) complexes: synthesis, spectroscopic characterization, X-ray structure determination, *in vitro* antibacterial activity and computational studies. *J. Mol. Struct.* 1196, 707–719. doi:10.1016/j.molstruc.2019.07.016
- Parlar, S., Sayar, G., Tarikogullari, A. H., Karadagli, S. S., Alptuzun, V., Erciyas, E., et al. (2019). Synthesis, bioactivity and molecular modeling studies on potential anti-Alzheimer piperidinehydrazide-hydrazones. *Bioorg. Chem.* 87, 888–900. doi:10.1016/j.bioorg.2018.11.051
- Parveen, S., Govindarajan, S., Puschmann, H., and Revathi, R. (2018). Synthesis, crystal structure and biological studies of new hydrazone ligand, 2- (Methoxycarbonyl-hydrazono)-pentanedioic acid and its silver (I) complex. *Inorganica Chim. Acta* 477, 66–74. doi:10.1016/j.ica.2018.02.022
- Patel, M. M., and Patel, L. J. (2014). Design, synthesis, molecular docking, and antibacterial evaluation of some novel fluoroquinolone derivatives as potent antibacterial agent. *Sci. World J.* 2014, 1–10. doi:10.1155/2014/897187
- Perontsis, S., Hatzidimitriou, A. G., Begou, O.-A., Papadopoulos, A. N., and Psomas, G. (2016). Characterization and biological properties of copper (II)-ketoprofen complexes. *J. Inorg. Biochem.* 162, 22–30. doi:10.1016/j.jinorgbio.2016.06.001
- Philip, J. E., Antony, S. A., Eeettinilkunnathil, S. J., Kurup, M. P., and Velayudhan, M. P. (2018). Design, synthesis, antimicrobial and antioxidant activity of 3-formyl chromone hydrazone and their metal (II) complexes. *Inorganica Chim. Acta* 469, 87–97. doi:10.1016/j.ica.2017.09.006
- Pisano, M. B., Kumar, A., Medda, R., Gatto, G., Pal, R., Fais, A., et al. (2019). Antibacterial activity and molecular docking studies of a selected series of hydroxy-3-arylcoumarins. *Molecules* 24, 2815. doi:10.3390/molecules24152815
- Popiolek, Ł., Piątkowska-Chmiel, I., Gawrońska-Grzywacz, M., Biernasiuk, A., Izdebska, M., Herbet, M., et al. (2018). New hydrazone-hydrazones and 1, 3-thiazolidin-4-ones with 3-hydroxy-2-naphthoic moiety: synthesis, *in vitro* and *in vivo* studies. *Biomed. Pharmacother.* 103, 1337–1347. doi:10.1016/j.biopha.2018.04.163
- Qiu, L., Lv, G., Guo, L., Chen, L., Luo, S., Zou, M., et al. (2015). Synthesis, crystal structure and antitumor effect of a novel copper (II) complex bearing zoledronic acid derivative. *Eur. J. Med. Chem.* 89, 42–50. doi:10.1016/j.ejmech.2014.10.028
- Quintanova, C., Keri, R. S., Chaves, S., and Santos, M. A. (2015). Copper (II) complexation of tacrine hybrids with potential anti-neurodegenerative roles. *J. Inorg. Biochem.* 151, 58–66. doi:10.1016/j.jinorgbio.2015.06.008
- Redgrave, L. S., Sutton, S. B., Webber, M. A., and Piddock, L. J. (2014). Fluoroquinolone resistance: mechanisms, impact on bacteria, and role in evolutionary success. *Trends Microbiol.* 22, 438–445. doi:10.1016/j.tim.2014.04.007
- Rocha, C. S., Bomfim Filho, L. F., De Souza, A. E., Diniz, R., Denadai, Â. M., Beraldo, H., et al. (2019). Structural studies and investigation on the antifungal activity of silver (I) complexes with 5-nitrofuranyl-derived hydrazones. *Polyhedron* 170, 723–730. doi:10.1016/j.poly.2019.06.033
- Santiago, P. H., Tiago, F. S., Castro, M. S., Souza, P. E., Martins, J. B., and Gatto, C. C. (2020). DFT analysis, spectroscopic study and biological activity of a newly synthesized benzoylhydrazone binuclear Cu (II) complex. *J. Inorg. Biochem.* 204, 110949. doi:10.1016/j.jinorgbio.2019.110949
- Sepay, N., and Dey, S. P. (2014). Synthesis and chemical reactivity of 4-oxo-4H-1-benzopyran-3-carboxaldehyde. *J. Heterocycl. Chem.* 51, E1–E24. doi:10.1002/jhet.2001
- Shabbir, A., Shahzad, M., Ali, A., and Zia-Ur-Rehman, M. (2014). Anti-arthritis activity of N'-[(2, 4-dihydroxyphenyl) methylidene]-2-(3, 4-dimethyl-5, 5-dioxidopyrazolo [4, 3-c] [1, 2] benzothiazin-1 (4H)-yl) acetohydrazide. *Eur. J. Pharmacol.* 738, 263–272. doi:10.1016/j.ejphar.2014.05.045

- Shankarwar, S. G., Nagolkar, B. B., Shelke, V. A., and Chondhekar, T. K. (2015). Synthesis, spectral, thermal and antimicrobial studies of transition metal complexes of 14-membered tetraaza [N4] macrocyclic ligand. *Spectrochimica Acta Part A Mol. Biomol. Spectrosc.* 145, 188–193. doi:10.1016/j.saa.2015.02.006
- Sherif, Y. E., and Hosny, N. M. (2014). Anti-rheumatic potential of ethyl 2-(2-cyano-3-mercapto-3-(phenylamino) acrylamido)-4, 5, 6, 7-tetrahydrobenzo [b] thiophene-3-carboxylate and its Co (II), Cu (II) and Zn (II) complexes. *Eur. J. Med. Chem.* 83, 338–343. doi:10.1016/j.ejmech.2014.06.038
- Soroceanu, A., Vacareanu, L., Vornicu, N., Cazacu, M., Rudic, V., and Croitori, T. (2016). Assessment of some application potentials for copper complexes of the ligands containing siloxane moiety: antimicrobial, antifungal, antioxidant and redox activity. *Inorganica Chim. Acta* 442, 119–123. doi:10.1016/j.ica.2015.12.006
- Sreepriya, R., Kumar, S. S., Sadasivan, V., Biju, S., and Meena, S. S. (2020). Synthesis, characterization and biological studies of Mn (II), Fe (III) and Co (II) complexes of (Z)-1, 5-dimethyl-4-(2-(2-oxopropylidene)hydrazinyl)-2-phenyl-1H-pyrazol-3(2H)-one. *J. Mol. Struct.* 1201, 127110. doi:10.1016/j.molstruc.2019.127110
- Stefani, C., Al-Eisawi, Z., Jansson, P. J., Kalinowski, D. S., and Richardson, D. R. (2015). Identification of differential anti-neoplastic activity of copper bis (thiosemicarbazones) that is mediated by intracellular reactive oxygen species generation and lysosomal membrane permeabilization. *J. Inorg. Biochem.* 152, 20–37. doi:10.1016/j.jinorgbio.2015.08.010
- Tian, W.-X., Yu, S., Ibrahim, M., Almonaofy, A. W., He, L., Hui, Q., et al. (2012). Copper as an antimicrobial agent against opportunistic pathogenic and multidrug resistant Enterobacter bacteria. *J. Microbiol.* 50, 586–593. doi:10.1007/s12275-012-2067-8
- Tolia, C., Papadopoulos, A. N., Raptopoulou, C. P., Psycharis, V., Garino, C., Salassa, L., et al. (2013). Copper (II) interacting with the non-steroidal antiinflammatory drug flufenamic acid: structure, antioxidant activity and binding to DNA and albumins. *J. Inorg. Biochem.* 123, 53–65. doi:10.1016/j.jinorgbio.2013.02.009
- Ugurulu, G., and Harmankaya, A. (2022). Investigation on molecular structure and electronic properties of zinc (II) complex with 2-acetylpyridinicotinichydrazone ligand. *Eurasia Proc. Sci. Technol. Eng. Math.* 20, 58–65. doi:10.55549/epstem.1222639
- Urquiza, N. M., Islas, M. S., Ariza, S. T., Jori, N., Medina, J. J. M., Lavecchia, M. J., et al. (2015). Anti-thyroid and antifungal activities, BSA interaction and acid phosphatase inhibition of methimazole copper (II) complexes. *Chemico-biological Interact.* 229, 64–72. doi:10.1016/j.cbi.2014.12.036
- Vanucci-Bacqué, C., Camare, C., Carayon, C., Bernis, C., Baltas, M., Nègre-Salvayre, A., et al. (2016). Synthesis and evaluation of antioxidant phenolic diaryl hydrazones as potent antiangiogenic agents in atherosclerosis. *Bioorg. Med. Chem.* 24, 3571–3578. doi:10.1016/j.bmc.2016.05.067
- Vieira, L. M. M., De Almeida, M. V., Lourenço, M. C. S., Bezerra, F. a.F., and Fontes, A. P. S. (2009). Synthesis and antitubercular activity of palladium and platinum complexes with fluoroquinolones. *Eur. J. Med. Chem.* 44, 4107–4111. doi:10.1016/j.ejmech.2009.05.001
- Yousefi, M., Sedaghat, T., Simpson, J., and Shafiei, M. (2019). Bis-aryolhydrazone based on 2, 2'-bis substituted diphenylamine for synthesis of new binuclear organotin (IV) complexes: spectroscopic characterization, crystal structures, *in vitro* DNA-binding, plasmid DNA cleavage, PCR and cytotoxicity against MCF7 cell line. *Appl. Organomet. Chem.* 33, e5137. doi:10.1002/aoc.5137
- Zülfiakaroglu, A., Ataol, Ç. Y., Çelikoğlu, E., Çelikoğlu, U., and İdil, Ö. (2020). New Cu (II), Co (III) and Ni (II) metal complexes based on ONO donor tridentate hydrazone: synthesis, structural characterization, and investigation of some biological properties. *J. Mol. Struct.* 1199, 127012. doi:10.1016/j.molstruc.2019.127012